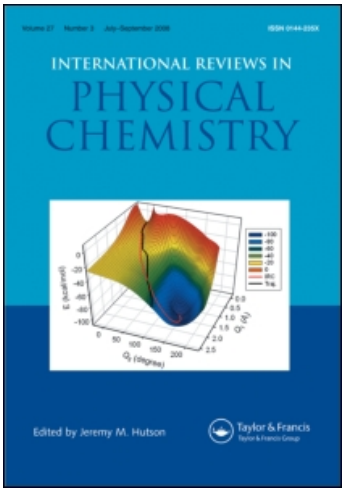

International Reviews in Physical Chemistry
Publication details, including instructions for authors and subscription information:
http://www.informaworld.com/smpp/title~content=t713724383

Surface photovoltage imaging for the study of local electronic structure at semiconductor surfaces

G. Haase

Online publication date: 26 November 2010

To cite this Article Haase, G.(2000) 'Surface photovoltage imaging for the study of local electronic structure at semiconductor surfaces', International Reviews in Physical Chemistry, 19: 2, 247 — 276
To link to this Article: DOI: 10.1080/01442350050020897
URL: http://dx.doi.org/10.1080/01442350050020897

INT. REVIEWS IN PHYSICAL CHEMISTRY, 2000, VOL. 19, NO. 2, 247–276

Surface photovoltage imaging for the study of local electronic structure at semiconductor surfaces

G. HAASE†
Department of Chemical Physics,
The Weizmann Institute of Science,
Rehovot 76100, Israel

Atomically-resolved surface photovoltage (SPV) imaging with a scanning tunnelling microscope was used by several laboratories to reveal the local degree of sub-surface electronic band bending at and around defects and adsorbates on various semiconductor surfaces. It turns out that the scanning tunnelling microscope tip-induced electric field, and/or the charging of surface states by the tunnelling current, can affect the band bending under the tip and help us learn more about the surface local electronic structure. This review features an explanation of the band bending phenomenon and how it gives rise to SPV, SPV imaging methods, a coverage of the experimental work done up to this date, and finally, a discussion about the source of atomically resolved features in the SPV maps.

1. Introduction

1.1. *What is surface photovoltage and what can it teach us?*

Thermal, as well as photogenerated electron–hole pair-mediated chemical reactions at semiconductor surfaces are very important in microelectronic processing and in photocatalysis, such as solar energy conversion and storage (Pichat and Fox 1988, Mills and Le Hunte 1997). It was found that these chemical processes are substantially affected by small amounts of defects or adsorbates at the semiconductor surface. Scanning tunnelling microscopy (STM) (see for example Güntherodt and Wiesendanger (1994)) combined with atomically-resolved local surface photovoltage (SPV) imaging, can provide a tool to study the electronic effects that are caused by a single defect, or a single adsorbate, and influence the chemistry at semiconductor–gas interfaces.

Most semiconductor materials have charge trapped on their surface at equilibrium conditions in the dark. The surface charge gives rise to a sub-surface electric field, which results in a sub-surface space charge region (SCR) (Bardeen 1947). The SCR is also known as a depletion or an accumulation layer, where the surface charge is compensated and the electric field is screened. The change in electric potential across the SCR gives rise to band bending. Since in most cases, the surface charge is due to trapped majority carriers (electrons for *n*-type and holes for *p*-type material), the bands are bent down for *p*-type and up for *n*-type semiconductor materials. Upon illumination of the sample with photons whose energy is larger than the bulk band gap, electrons and holes are formed. The photogenerated charge carriers can separate in the sub-surface electric field and undo the band bending. This results in a non-equilibrium build up of a *surface photovoltage* (SPV) between the illuminated surface and the dark back of the sample, which equals the change in the degree

† Email: gad.haase@weizmann.ac.il

International Reviews in Physical Chemistry ISSN 0144-235X print/ISSN 1366-591X online
http://www.tandf.co.uk/journals

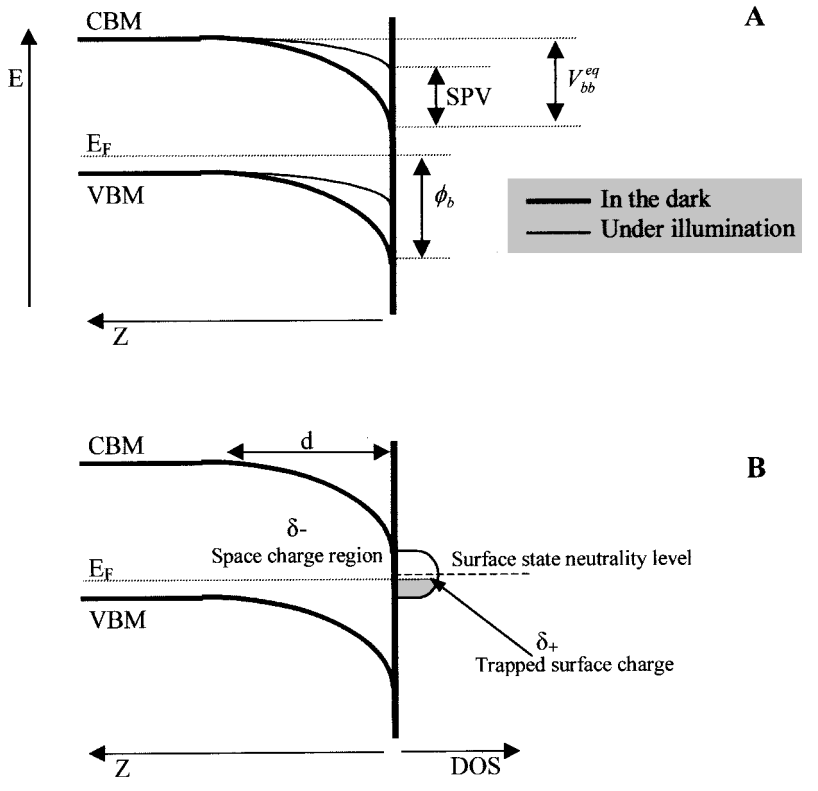

Figure 1. A schematic view of the band energy diagram for a *p*-type semiconductor, as a function of Z, the distance from the surface into the bulk. (*a*) An illustration of the SPV, V_{bb}^{eq} (the degree of band bending in equilibrium), and ϕ_b (the majority carrier barrier) quantities. E_F is the Fermi level. (*b*) An illustration of Fermi level pinning and band bending due to trapped charge in a surface state band. d is the SCR depth.

of band bending (see figure 1 (*a*)). A sufficiently high density of photocarriers can flatten the bands and give rise to a SPV that equals the original band bending in equilibrium (in the dark).

The charge traps are surface states that overlap the bulk semiconductor band gap. They stem from the termination of a three-dimensional lattice (Tamm 1932) and/or from dangling bonds, defects, or adsorbates (Moench 1993). Their charge, and the effect of its electric field on the electronic structure in their vicinity, can have a major influence on the local chemical reactivity at semiconductor surfaces. Local changes in the work function as a result of local band bending can affect charge transfer between the surface and an adsorbate. In addition, surface states can screen external electric fields that would otherwise also give rise to band bending, thus possibly affecting cross-sections for photochemistry of adsorbed species: photo-excited electrons in the semiconductor substrate can couple to the adsorbate by exciting a transient negative ion state, which decays back to a neutral with vibrational excitation that can lead to bond-breaking (Gadzuk 1999). This process is crucially dependent on the lifetime of the electron in the adsorbate. The lifetime, in turn, is dependent on the degree of band bending caused by the adsorbate's temporary charge, since it controls the

adsorbate–substrate states' overlap. In this review we hope to show that imaging the SPV on the sub-nanometre scale with a scanning tunnelling microscope can help us understand the local electronic structure and its influence on the local reactivity around defects and adsorbates at semiconductor surfaces. SPV imaging at surfaces of semiconductor devices can also help us understand the structure of junctions as well as electron dynamics (Glembocki *et al*. 1992).

The phenomenon of surface-state-induced band bending can be illustrated by the following example: suppose we have dangling bonds at a surface that must contain one electron per one unsaturated bond to maintain surface neutrality, and the energy band due to their two-dimensional lattice is centred at some energy inside the bulk band gap (see figure 1 (*b*)). If the semiconductor material is *p*-type doped and the bands are flat, its Fermi level is close to the valence band maximum (VBM) deep in the bulk. If the bulk bands were flat, the surface state band neutrality level would end up above the Fermi level and hence the surface band will be positively charged. The positive charge, in turn, causes the bands to bend downward, lowering the surface state energy with respect to the Fermi level and thus, diminishing the surface charge. At equilibrium, the remaining positive charge per unit surface area, Q_{ss}, is fully compensated by the charge of the negative ionized dopant atoms in the SCR that is depleted from holes (also called the depletion layer): $Q_{ss} = qN_d d$, where q is the elementary electron charge, N_d is the dopant concentration per unit volume (acceptor for *p*-type samples), and d is the SCR, or the depletion layer depth. The resulting surface potential, or the degree of band bending V_{bb}, is very sensitive to Q_{ss}. In the full depletion approximation, it is given by:

$$V_{bb} = \frac{qN_d d^2}{2\varepsilon},$$

here ε is the permittivity of the bulk semiconductor. The Fermi level ends up close to the neutrality level of the surface state band, and hence it is referred to as 'pinned' by this surface state. The pinning concept describes two phenomena: (a) the Fermi level energy with respect to the band edges at the surface is independent of doping (i.e. of E_F–VBM in the bulk), and (b) it is insensitive (to a degree) to the exertion of external electric field. Small changes in the Fermi level energy with respect to the band edges, and hence with respect to the surface band neutrality level, result in changes of the surface charge that can screen external electric fields.

While a typical depletion layer depth is of the order of several tens of nanometres, the lateral spread of the potential change at the surface, around a single charged feature, can be smaller by an order of magnitude. Surfaces such as the Si(111)7 × 7 surface, which are 'metallic', or have their bulk band gap covered with surface states bands due to dangling bonds (Hamers *et al*. 1986a, b), can screen laterally an electric field from a charged adsorbate very efficiently. As a result, the adsorbate-induced band bending, and hence the SPV variations, are expected to be confined to a small (< 1 nm) region at the surface (see section 4). As we will show later, there are other effects that confine the SPV signal to subnanometre-diameter areas, and therefore, justify even further the use of STM for SPV imaging with a 1 Å lateral resolution.

Upon illumination with photons whose energy exceeds the band gap, electrons and holes that are photogenerated in the semiconductor bulk are subjected to the sub-surface electric field. Photocarriers of the opposite sign to that of the trapped surface charge drift toward the surface, and consequently, reduce the band bending. Yet the bands are never flattened completely since as the surface potential V_{bb}

becomes closer to zero, the barrier for the other carrier type to reach the surface is reduced. A steady state is established under illumination when both carrier types arrive at the surface with equal fluxes and recombine there. Thus the magnitude of the SPV, or the change in V_{bb} due to illumination, depends on several factors (Darling 1991, Aphek *et al.* 1998), such as the carriers' surface recombination velocity, the temperature, the light intensity and absorption depth (or wavelength). Increasing the light intensity or decreasing the surface recombination velocity will asymptotically decrease the band bending and make the SPV approach its maximum value, which equals V_{bb}^{eq} in the dark. Since the light intensity has to be maintained below the damage threshold, we are mainly dependent on the choice of surface in having the SPV value approach the degree of band bending in the dark. For example, the high recombination rate at Si(111)7×7 surfaces due to the high density of surface states that cover the bulk band gap, limits the SPV to less than half of V_{bb}^{eq}. On the other hand, the lack of surface states on clean and defect-free GaAs(110) surfaces, allows the bands to flatten almost completely upon a relatively weak illumination.

1.2. *Evaluation of the SPV magnitude*

Without loss of generality, we will refer here to the more common case where the surface charge is due to the majority carrier being trapped at the surface in equilibrium (in the dark). In this case, the SCR that screens the surface charge is due to a depletion layer. Illumination with super-band-gap photons creates electrons and holes in equal number. The photocarriers redistribute so that the minority carriers move toward the surface and lower the trapped surface charge, thus reducing the band bending. However, the equilibrium band bending will be reduced even if the equilibrium surface charge is not changed by illumination, as a result of the screening of the electric field from the surface (or from any external source) by the photocarrier distribution (Johnson 1958). In any case, the band bending should approach zero as the photogenerated carrier concentration is increased, bringing the SPV value closer to V_{bb}^{eq} (Aphek *et al.* 1998).

In the dark, the majority carrier thermal emission rate above the surface barrier ϕ_b (the energy difference between the conduction band minimum (CBM) and the Fermi level for *n*-type samples, and between the Fermi level and the VBM for *p*-type samples, at the surface, see figure 1 (*b*)) is:

$$j_{maj} = A^* T^2 \exp\left(-\frac{\phi_b}{k_b T}\right),$$

where A^* is the effective Richardson constant, k_b is the Boltzmann constant and T is the temperature (Sze 1981). Steady state conditions under illumination of a sample with a fast carrier recombination rate at its surface requires that the extra majority carrier flux j_{maj}^{ph} which can cross the reduced barrier $\phi_b - q|SPV|$ equals the photogenerated minority carrier flux j_{min}^{ph} at the surface (Hecht 1990, Cahill and Feenstra 1993):

$$j_{min}^{ph} = j_{maj}^{ph} = A^* T^2 \exp\left(-\frac{\phi_b}{k_b T}\right)\left(\exp\left(\frac{q|SPV|}{k_b T}\right) - 1\right)$$

or

$$SPV = \frac{k_b T}{q} \ln\left(1 + \frac{\exp(\phi_b / k_b T)}{A^* T^2} \beta P\right),$$

where $j_{\min}^{\mathrm{ph}} = \beta P$ is the photogenerated minority carrier flux at the surface, P being the laser power and β a proportionality factor which is dependent on the photon flux at the surface, sample reflectivity, the photon absorption depth, carrier mobilities, etc. Hamers and Markert (1990), in the first paper that described local SPV imaging with a scanning tunnelling microscope, fit the SPV measured on a Si(111)7 × 7 surface as a function of laser power, P, to the expression $SPV = A \ln(1 + BP)$. They obtained a very good fit which yielded $A = 30.6\,\mathrm{mV}$ (close enough to $k_{\mathrm{b}}T/q = 26\,\mathrm{mV}$ at $T = 300\,\mathrm{K}$).

When the surface recombination velocity is low or negligible, the reduction in the band bending upon illumination can be estimated by defining separate non-equilibrium quasi Fermi levels for electrons and for holes (Garrett and Brattain 1955). If the carrier diffusion length is large with respect to the depletion layer width, these quasi Fermi levels may be approximated as position-independent (flat) throughout this region. The full derivation of the expression for the SPV in this case is given in a comprehensive review by Kronik and Shapira (1999).

Finally, since electrons diffuse faster than holes, a small photo-induced positive surface potential for both *n*- and *p*-type samples, named the Dember (1931) potential, results from the larger loss of photo-electrons into the bulk. The potential that builds up compensates for the diffusion constant inequality and makes the electron and hole fluxes at the surface identical in steady state. The Dember SPV, which does not stem from band bending in the dark, is of the order of a few mV only.

2. Experimental methodology

The only measurable quantity that a STM can detect is the tunnelling current. Thus, the greatest difficulty in obtaining an accurate measurement of the local SPV stems from correlating correctly the surface potential to the tunnelling current. In addition, one has to bear in mind that the measured SPV reflects not only the equilibrium sub-surface electric field in the dark for an unperturbed sample, but also the influence of the STM tip on the band bending.

2.1. *Methods for 'metallic' surfaces*

A 'metallic' surface is defined as a surface with a continuum of overlapping surface state bands which cover the whole band gap. An I–V curve taken with the STM at any location on such a surface will constitute a homogeneously rising function and will give zero tunnelling current only at zero bias voltage.

A classical example is that of the Si(111)7 × 7 surface, which according to the dimer adatom stacking-fault (DAS) model (Takayanagi *et al.* 1985, Hamers *et al.* 1986b, Tromp *et al.* 1986), has dangling bond states covering the whole band gap. Thus all the SPV imaging using the following method were done on Si(111)7 × 7 surfaces. Figure 2 (taken from Hamers and Markert (1990b)) show two I–V curves that were taken on a clean Si(111)7 × 7 surface in the dark and under illumination with photon energy that exceeds the band gap (from a He–Ne laser). The bias, V, is supplied to the dark back of the sample. The two I–V curves meet at a sample bias value of +1.2 V since in both cases, the set point was chosen to be 1 nA at this bias. However, at any other bias the curves depart, and the bias for which the tunnelling current zeroes under illumination is no longer zero. Since the surface potential with respect to the tip has to be zero when no net current flows across the tunnel junction, the non-zero bias that gives rise to zero current, $V_{\mathrm{s}}(I_{\mathrm{tun}} = 0)$, indicates that a potential difference was built under illumination between the dark

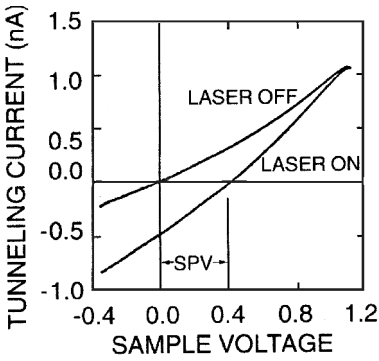

Figure 2. I–V curves with and without illumination from a He–Ne laser, taken on a clean p-Si(111)7 × 7 surface, starting at I_{tun} = 1 nA at V_s = 1.2 V (taken from Hamers and Markert (1990a, b), with permission).

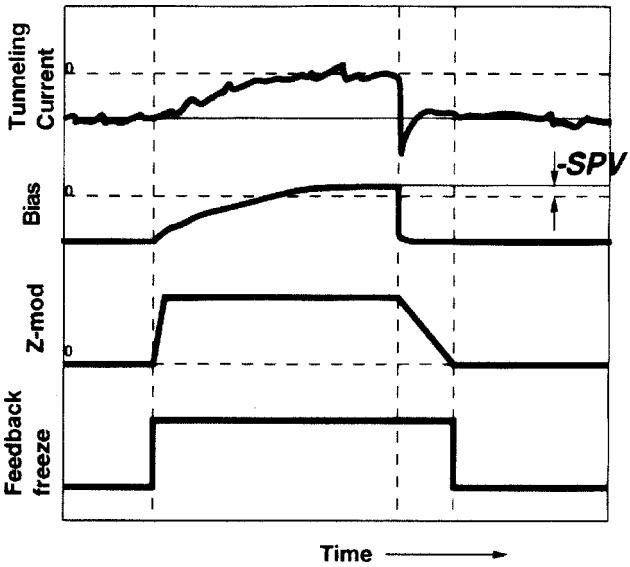

Figure 3. A schematic plot of the tunnelling current, sample bias, tip Z-position modulation (used in Gorelik *et al.* (1998)), and CCT feedback disabling control as a function of time, in a typical SPV imaging using the current nulling technique.

side of the sample to its illuminated surface under the tip and that its value is SPV = $-V_s(I_{tun} = 0)$.

Most of the work reported in the literature of SPV imaging of Si(111)7 × 7 surfaces with STM (Hamers and Markert 1990a, b, Kuk *et al.* 1990, 1991, Gorelik *et al.* 1998) is based on the interruption of the constant-current (z-control) feedback loop at every effective pixel for a short time interval, in which a second feedback loop was employed to search the sample bias that nulls the tunnelling current. Figure 3 shows a schematic plot of the various signals as a function of time. The final sample bias, before it is restored to the topography imaging value, is held until the next cycle and fed to an additional analogue-to-digital channel, to be displayed side by side next to the constant current topography (CCT) image.

Due to the low density of states, and hence the small gradient of the I–V curves near zero surface potential, a few minor variations were adapted: amplification of the current, to aid the determination of the zero current point within the noise, can be achieved by using a lower sample bias magnitude or setting the tunnelling current to a higher value during the acquisition of the topography, so as to force the tip to be closer to the sample. A different approach, as is demonstrated in figure 3, was to push the tip position closer to the surface while the CCT feedback is turned off (Gorelik *et al.* 1998). Bringing the tip closer to the surface by 0.8 Å yielded an accuracy of ± 2 mV in the measured SPV value. Another approach was based on the assumption that the I–V curves are nearly linear in a small enough interval around $V_s(I_{tun} = 0)$. Here, the bias that gives rise to a current of 40 pA, which could be safely determined above the noise level, was found, and by taking an additional current measurement at a different bias (higher by up to 30 mV), the $V_s(I_{tun} = 0)$ could be extrapolated (Kochanski and Bell 1992).

The current nulling method of local SPV measurement is the most accurate method among the ones reported so far, as it evaluates the SPV while no current flows across the junction, as will be discussed later on. However, it is limited to 'metallic' surfaces and it does not allow the study of bias or non-zero current effects, which proved to add valuable information about the nature of the local surface electronic structure.

2.2. *Methods for SPV determination at non-zero tunnelling current*

Non-'metallic' non-degenerate semiconductor surfaces do not exhibit one single bias value that zeroes the tunnelling current, due to an energy gap between the filled and the empty states. As a result, the measurements have to be performed at bias values where tunnelling current exists, and can reflect changes in the surface potential upon illumination.

The first method which was used by Cahill and co-workers (Cahill and Hamers 1991a, b, 1992, Cahill and Feenstra 1993), employed modulation of the surface potential by two sources, operating at two different frequencies, above the CCT feedback frequency cut-off: one source is a SPV modulation due to chopped laser illumination of the surface under the tip, and the other source is a sinusoidal bias modulation (typically 30 mV RMS) supplied to the dark back of the sample. The two components of the resulting tunnelling current modulation (ΔI_{bias} due to the bias modulation and ΔI_{SPV} due to the chopped illumination) were detected with two lock-in amplifiers. The SPV value was taken as $(\Delta I_{SPV}/\Delta I_{bias})\Delta V_s$, where ΔV_s is the applied sample bias modulation amplitude.

The 'double modulation' method assumes linear I–V curves, and hence may be accurate for small SPV values only, where it was shown that the correction terms are negligible. In addition, a cross-talk between the two frequency detection channels (mainly due to the abrupt changes in the SPV) is neglected. As a result, although this method yielded much valid data, mainly for Si(001)2×1 surfaces, the following 'bias compensation' technique was developed (McEllistrem *et al.* 1993, Aloni *et al.* 1999, Gorelik *et al.* 1999).

Once more, the sample was illuminated under the tip with chopped light. The tunnelling current as a function of time is depicted in curves b and c in figure 4, where the light-on and the light-off intervals are shown in curve a. When the light intensity was too high (typically > 500 mW cm^{-2}, curve b), heating and cooling of the sample and the tip gave rise to an increase and decrease in the absolute value

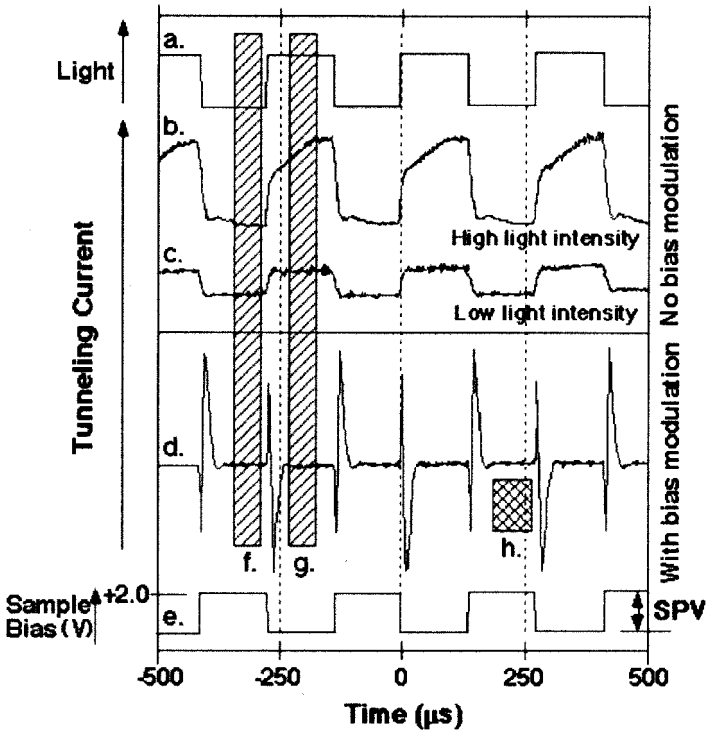

Figure 4. SPV imaging using the bias-compensation technique for n-Si(001)2 × 1 surface under $V_s = +2$ V. Traces of the light intensity (curve a), tunnelling currents at high (curve b) and low (curve c) illumination intensity with no bias modulation, current at low light intensity with bias modulation (curve d), and the modulated sample bias (curve e), are depicted as a function of time. The bars f and g represent the tunnelling current averaging windows at the light-on and light-off periods, respectively, and the bar h shows the time period when the CCT feedback was enabled.

of the tunnelling current, respectively, with time. Thus, one has to either restrict the light intensity at the surface or increase the light chopping repetition rate.

Next, the sample bias was altered during the light-on period so as to compensate for the SPV and bring the tunnelling current back to its value in the dark. The tunnelling current was averaged over sampling windows, during both light-off and light-on periods, as indicated by boxes f and g, respectively, and held separately. The difference between the light-on and the light-off current signals was nulled by a feedback loop which determined the sample bias modulation amplitude, V_{mod}. In other words, the surface potential, $V_{surf} = V_s + V_{mod}F(t) + \mathrm{SPV}F(t)$, where $F(t)$ is 0 at light-off and 1 at light-on periods, was kept constant. Curve d shows the resulting tunnelling current waveform, as a result of the bias waveform that is depicted in curve e. All curves in figure 4 were taken for an n-Si(001)2 × 1 surface under a sample bias of +2 V, where the SPV happens to be positive and hence the tunnelling current increases in the light-on periods. Box h in figure 4 indicates the time window in which the constant current (topography) feedback loop was enabled during the dark periods only. Spikes on the tunnelling current due to capacitive coupling between the sample and the tip set the limit to the highest possible repetition rate, which varied between 3 and 5 kHz, much above the topography feedback frequency cut-off

(~1 kHz) and far enough below the current detection system response (30 kHz). The capacitive spikes were minimized by feeding the inverted sample bias waveform to the tip through a 0.2 pF capacitor. Obviously, the current sampling windows f, g and h were chosen so as to avoid these spikes. The SPV value, which is the inverted bias modulation amplitude (SPV = $-V_{\mathrm{mod}}$) was imaged simultaneously with the constant current topography.

2.3. *Decay time of the SPV signal*

Upon the switching on of a super-band-gap illumination, the band bending, or the SPV, arrives at its steady state value within < 1 ns. However, after the light is switched off, it takes time for the majority carriers to cross the gradually increasing Schottky barrier, and restore the original value of the trapped surface charge. Hence, the SPV decay time, τ, increases gradually as the SPV decreases. The total decay time, τ_{D}, is related to the initial decay time through the expression (Hamers and Cahill 1991)

$$\tau(t = 0) = \tau_{\mathrm{D}} \exp[-qSPV(t = 0)/k_{\mathrm{b}}T] .$$

At Si(111)7 × 7 surfaces, where Fermi's golden rule and the continuous density of states that cover the bulk band gap give rise to a fast carrier recombination velocity, the SPV decay time was evaluated as $\tau_{\mathrm{D}} = 1\,\mu\mathrm{s}$, using a time correlation technique with a scanning tunnelling microscope (Hamers and Cahill 1991). However, on large, clean and perfect semiconductor surfaces with no surface states in the bulk band gap, it often takes minutes to days for the SPV to decay, depending on the band gap. Such a long relaxation time renders the double-modulation and the bias-compensation methods useless. For example, the SPV relaxation time on a GaAs(110) surface (no surface states, band gap of 1.4 eV), produced by cleavage of an undoped GaAs bar, may last a few minutes. Nevertheless, in our work on cleaved 350 μm thick GaAs wafers, it seemed that the SPV decayed to at least 10% of its value during illumination within some 50 μs after the light was shut off. We do not know whether to attribute it to the small thickness of the sample (and hence, a nearby large area of (100) surface where recombination is fast) or to tip-induced recombination. Surely, when one works with a *p*-type sample under a negative sample bias (or *n*-type under positive bias), which is a common mode of work as will be shown later (section 3.3), the tip injects majority carriers into the surface, which should hasten the decay of the SPV signal in the dark.

2.4. *STM tip-induced changes in SPV*

2.4.1. *Tunnelling current effects*

Figure 5 shows the effect of the tunnelling current on the SPV values, as obtained by Cahill and Feenstra (1993) for Si(111)2 × 1 surfaces; the injection of minority carriers by the tip into the sample reduces the steady state surface charge in the dark, giving rise to a lower magnitude of band bending, and consequently, a lower SPV. Conversely, the injection of majority-type carriers to the surface can slightly increase the surface charge in the dark and hence, increase the SPV magnitude.

A good example for current-induced localized SPV features can be viewed on Si(001)2 × 1 surfaces. On these surfaces, the upper most Si atoms are arranged in dimer rows (Hamers *et al.* 1986a) that give rise to an energy gap between the filled π and the empty π^* dimer-induced surface states (Himpsel and Fauster 1984, Hamers *et al.* 1987, Hamers and Köhler 1989). Figure 6 shows topography ((*a*)

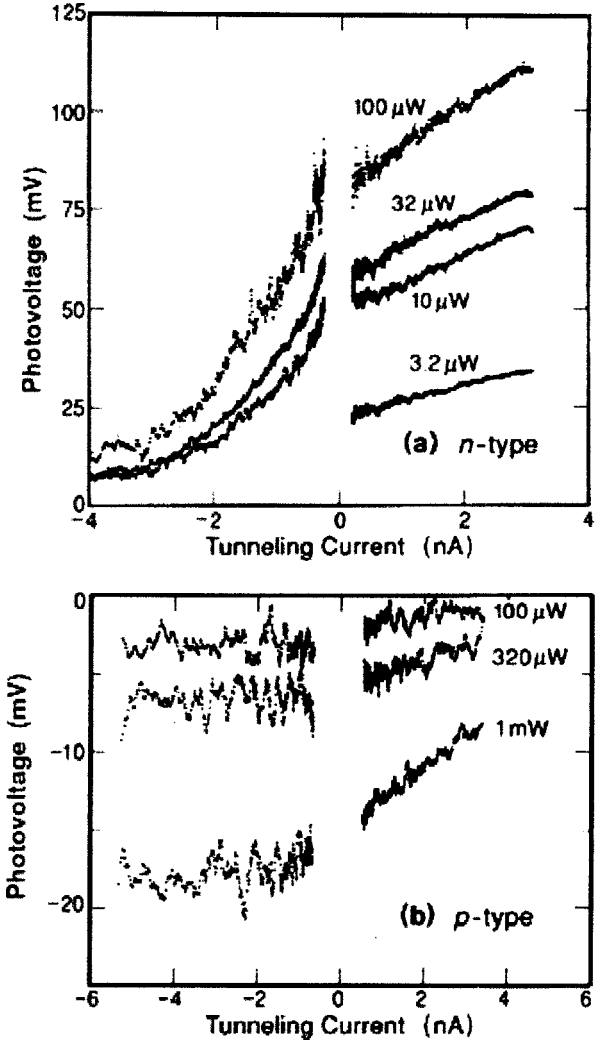

Figure 5. Measured SPV versus tunnelling current for (*a*) *n*- and (*b*) *p*-type Si(111)2 × 1 surfaces, for various laser power. The sample bias is −1.8 V and +1.8 V for negative and positive currents, respectively, in (*a*), and −2 V and +2 V in (*b*). (Reproduced with permission from Cahill and Feenstra (1993).)

and (*c*)) and SPV ((*b*) and (*d*)) images of *n*-Si(001)2 × 1 at V_s = 1.2 V, taken with the bias compensation method, for I_{tun} = 1 nA ((*a*) and (*b*)) and I_{tun} = 0.3 nA ((*c*) and (*d*)) (Hamers *et al*. 1992). In the SPV images, bright shades correspond to a higher (more negative) SPV magnitude. These images are very similar to those obtained with the double modulation technique by Cahill and Hamers (1991a). They show a strong enhancement of the observed SPV, giving rise to sub-nanometre features at the C-type defects (Hamers and Köhler 1989), and the B-type steps that run perpendicularly to the dimer rows at the upper terrace, as the set tunnelling current is increased. On the other hand, missing dimer defects showed no SPV enhancement.

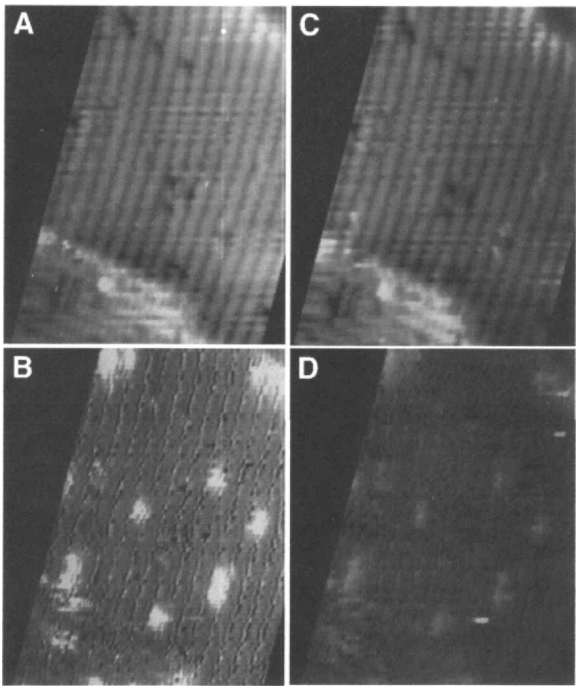

Figure 6. (*a*), (*c*) Topography and (*b*), (*d*) SPV images of *n*-Si(001)2 × 1 at $V_s = -1.2$ V, taken with the bias compensation method, for $I_{tun} = 1$ nA (A,B) and $I_{tun} = 0.3$ nA (C,D). In the SPV images, bright means higher negative SPV magnitudes (Hamers *et al*. 1992). The same grey scale is used for both (*b*) and (*d*) SPV maps.

Type-B steps and type-C defects were shown to add localized surface states in the energy gap between the π and the π^* states on the Si(001)2 × 1 surface (Hamers and Köhler 1989, Cahill and Hamers 1992). Longer lifetime of the charge, injected from the scanning tunnelling microscope tip, in the latter isolated states, can bring about surface charging when the tip is placed above these defect locations. Naturally, the steady state charge is proportional to the set tunnelling current, and it should cause band bending in its vicinity only when the tip is positioned precisely over these isolated surface states. This explains the sub-nanometre scale of the observed SPV features in figure 6. Note that the SPV, both on the clean surface and on top of the type-B steps and type-C defects, was current dependent (images (*b*) and (*d*) use the same grey scale). Cahill and Hamers (1992) estimated the lifetime of an injected hole from the tip (at $V_s < 0$) as 10^{-10} s on the Si dimers, while at type-B steps and type-C defects it is larger by a factor of two.

2.4.2. *Tip-induced electric field effects*

The displacement vector component perpendicular to the surface, outside the semiconductor, $\mathbf{D}_{ext}$, and immediately beyond the surface inside the bulk semiconductor, $\mathbf{D}_0$, must satisfy the relation: $\mathbf{D}_{ext} = \mathbf{D}_0 + Q_{ss}$, where Q_{ss} is the surface charge density. If no surface states are present around the Fermi level energy, and hence there is no surface charge ($Q_{ss} = 0$), then $\varepsilon_0 \mathbf{E}_{ext} = K_s \varepsilon_0 \mathbf{E}_0$ (where K_s is the dielectric

constant of the bulk). The electric field in the bulk, right beyond the surface is:

$$\mathbf{E}_0 = \left(\frac{2N_d q}{K_s \varepsilon_0} V_{bb}\right)^{1/2}$$

and the electric field between the tip and the sample (assuming that they have similar work function values) is:

$$\mathbf{E}_{ext} = \frac{V_s - V_{bb}}{s},$$

where V_s and V_{bb} are the bias of the *back* of the sample with respect to the tip and the band bending, respectively, and s is the tip–sample separation. The tip is treated as a flat sheet of metal that is parallel to the surface. For a positive sample bias,

$$V_{bb} = C\left(1 - \left(1 + \frac{2V_s}{C}\right)^{1/2}\right) + V_s,$$

$$C = s^2 \frac{K_s N_d q}{\varepsilon_0}.$$

For example, for GaAs with $N_d = 10^{17}\,\mathrm{cm}^{-3}$, and taking $s = 10\,\text{Å}$, we obtain $C = 0.024\,\mathrm{V}$; out of 1 V sample bias, 0.8 V can fall inside the semiconductor when one images the surface state free GaAs(110) surface. In fact, the tip can induce a great deal of band bending (Feenstra and Stroscio 1987, Weimer *et al.* 1989), up to a point where the Fermi level meets a surface state or a band edge, where charge can accumulate and screen much of the tip's electric field.

Figure 7 shows the SPV as a function of sample bias (Hamers *et al.* 1992, McEllistrem *et al.* 1993), averaged on clean, defect-free regions of *n*- and *p*-type Si(111)7 × 7, Si(100)2 × 1 and Si(111):H surfaces, using the bias compensation method. The measurements where done with a tunnelling current of 0.3 nA, where the SPV did not appear to be current dependent. On the surface-state–free hydrogen-terminated Si(111):H surfaces (Higashi *et al.* 1990), as is illustrated in figure 8 for an *n*-type material, the bands are free to bend until the Fermi level hits the bulk bands projection at the surface. Since the carrier recombination rate is low on this surface, the measured SPV reflects almost the entire large tip-induced band bending, except for the anomalous case of the *p*-Si(111):H surface at negative sample bias, which will be discussed later.

Si(001)2 × 1 surfaces have the dimers, filled π and empty π^* bands, positioned beneath the valence band maximum (VBM) and inside the band gap beneath the conduction band minimum (CBM), respectively (Himpsel and Fauster 1984, Hamers *et al.* 1987) (see figure 8). As a result, the Fermi level energy at the surface has to be confined between these bands. For *n*-type samples, the bands are always bent upward, giving rise to a positive SPV. At positive sample bias, the bands can be bent further up until the Fermi level meets with the π state, or the VBM, producing SPV values that respond to the bias as in the *n*-Si(111):H case. However, at the *p*-Si(001)2 × 1 surface, the bands are free to bend some $\pm 0.2\,\mathrm{eV}$, giving rise to a small value of positive SPV at $V_s > 0$ and negative SPV at $V_s < 0$.

Finally, at Si(111)7 × 7 surfaces the Fermi level is pinned close to the centre of the band gap (Himpsel *et al.* 1983, Demuth *et al.* 1986, Hamers *et al.* 1986b). For 0.1 Ω cm Si samples, the equilibrium degree of band bending is about 0.45 eV downward for *p*- and upward for *n*-type material. However, the observed SPV magnitudes, depicted in figure 7, are substantially lower than 0.45 V due to the

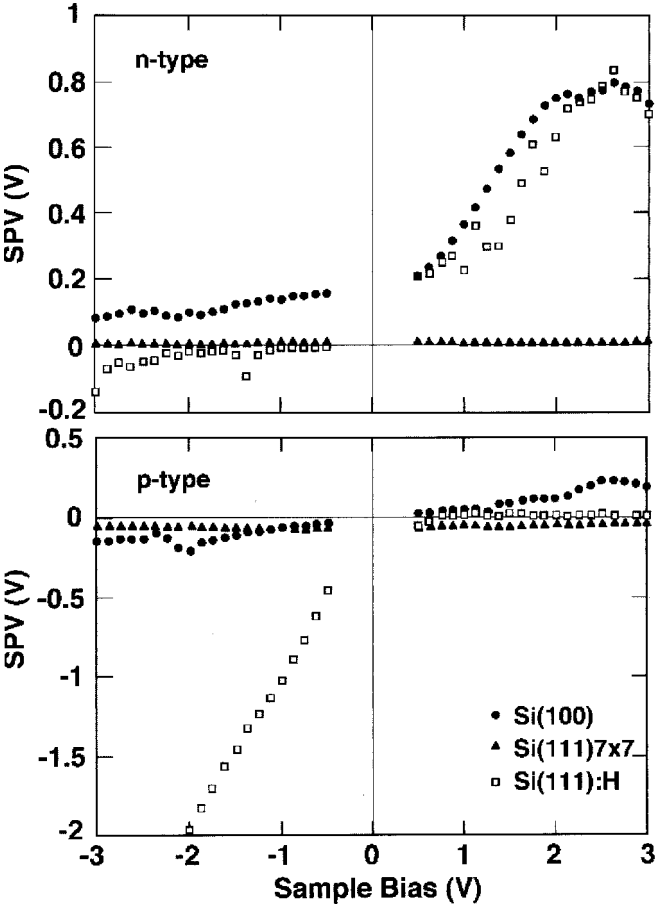

Figure 7. Measured SPV versus sample bias for *n*- and *p*-type Si(111)7 × 7, Si(100)2 × 1, and Si(111):H surfaces, at I_{tun} = 0.3 nA using the bias-compensation technique.

high recombination velocity at this surface. Nevertheless, the SPV values were not dependent on the sample bias, indicating that the surface states screen the external field efficiently.

It is important to note that the electric field in the sample–tip junction does not depend solely on the bias, but also on the sharpness of the tip and its composition. A contact potential difference, due to different work function values of the sample surface and the tip apex, adds to the electric field. Also, the tip surface distance is bias dependent, and the electric field is strongly dependent on this distance (Weimer *et al.* 1989); the tip–sample separation shrinks substantially when the bias values are inside the forbidden gap, and may yield a very high electric field that can cause the Fermi level to penetrate deeply into surface states or surface resonances (Aloni and Haase 1999).

Adsorbates or defects that change locally the surface density of states can vary locally the degree of tip-induced electric field penetration into the semiconductor, and hence, change the band bending and the resulting local SPV. Oxygen at Si(111)7 × 7 surfaces is an example of an adsorbate that lowers the density of states on a surface

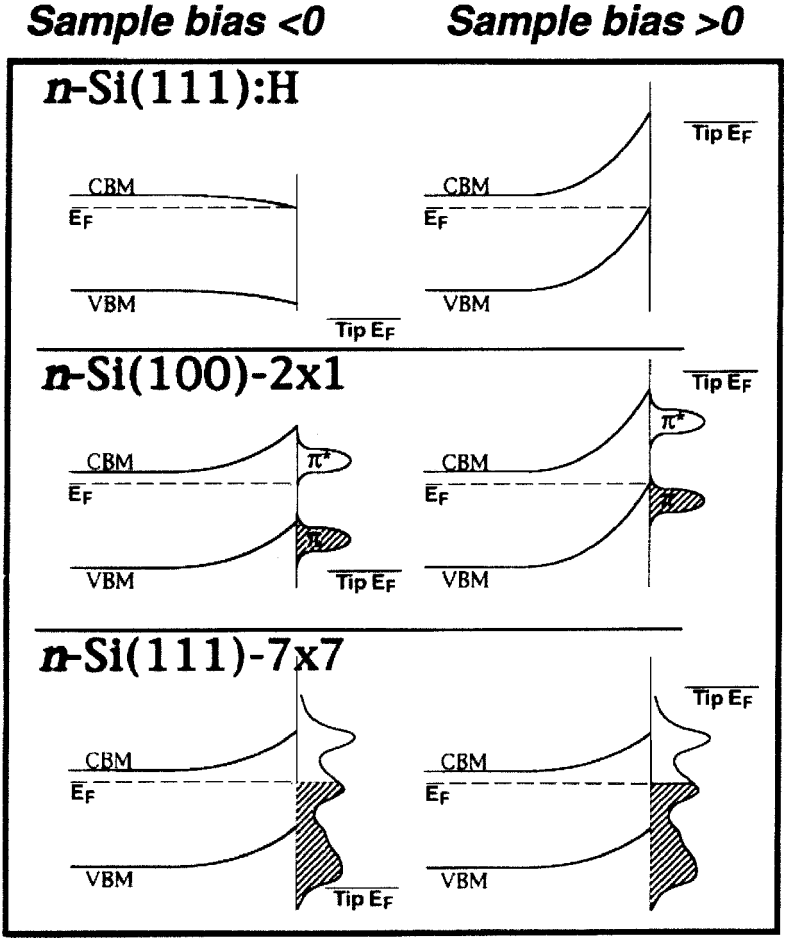

Figure 8. A schematic view of the expected maximum allowed tip-induced band bending for positive and negative sample bias, for *n*-type Si(111)7 × 7, Si(100)2 × 1, and Si(111):H surfaces.

that otherwise pins the Fermi level (McEllistrem *et al.* 1993) (see section 3.1.2), while a Cs adatom at GaAs(110) or Si(001)2 × 1 surfaces is an example of an adsorbate that locally pins the Fermi level at a surface with an energy gap (Aloni *et al.* 1999, Gorelik *et al.* 1999) (see sections 3.3.2 and 3.2.2).

Figure 9 illustrates the effect of a single isolated dangling-bond surface state, on a surface that otherwise has no surface states in the bulk band gap. It shows a solution of the Poisson equation in cylindrical coordinates for a single 2-electron localized surface state, on a 'smooth' GaAs(110)-like surface (no surface states elsewhere): **r**, is the distance from the localized surface state parallel to the surface, and **z** is the distance into the *p*-GaAs-like bulk. The local density of the surface state was shaped as a Gaussian, centred at 0.56 eV above the VBM with a full width at half maximum (FWHM) of 0.2 eV, and defined neutral when half filled (occupied with 1 electron). The single (2 electron) surface state was localized in a cylinder of 2 Å radius and 2 Å height at **r** = **z** = 0. The tip-induced electric field was introduced through the positioning of a flat 'conductor' at a bias of +2.5 V (figure 9 (*a*)) or +0.3 V (9 (*b*)) with

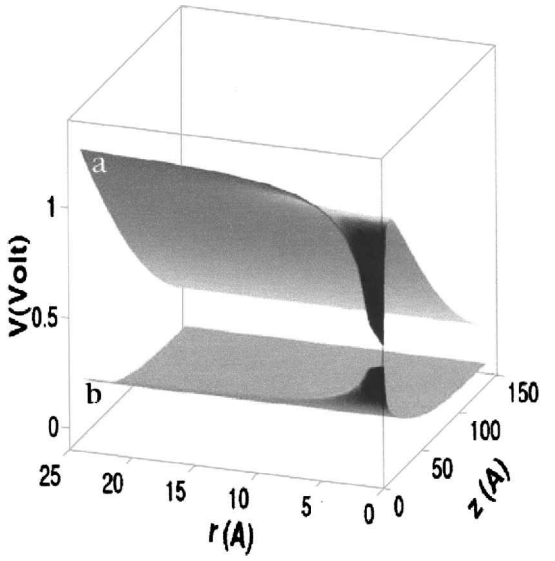

Figure 9. A numerical solution of the Poisson equation, showing the electrical potential (V) as a function of the distance into the bulk (z) and the lateral distance (r) for a surface-state (0.54 eV above VBM, at $r = z = 0$) on p-GaAs(110) surface, with tip bias of (*a*) 2.5 V and (*b*) 0.3 V. See text for details.

respect to the back of the GaAs sample ($z = 600$ Å), parallel to the sample surface and 12 Å away from it. At a lateral distance away from the localized surface state (large **r**), the electric potential increases (downward band bending) as **z** decreases, due to the penetration of the tip-induced electric field into the sample. However, at **r** = 0, the Fermi level is locally pinned very close to the state's neutrality energy, thus keeping the degree of band bending nearly independent of the sample–tip bias. Hence the SPV is expected to be strongly bias (and tip shape) dependent everywhere except on top of such a dangling bond.

2.4.3. *Possible errors and artifacts*

As was mentioned earlier, the main errors in a SPV measurement with a scanning tunnelling microscope stem from the fact that the surface potential has to be evaluated from the change in tunnelling current due to illumination. Obviously, any change in current that does not arise from the photo-induced band flattening can give rise to wrongly observed SPV values. An example is the case of p-type samples with low surface recombination velocity, which are imaged at negative sample bias. Figure 10 shows schematically that photo-generated electrons (minority carriers) in the conduction band can tunnel directly into the tip (arrow #2). In fact, since the tunnelling barrier that electrons in the conduction band face is lower than the barrier for electrons in the valence band (by 1.1 eV for Si), and since the current is exponentially dependent on the barrier height, the conduction band photoelectrons contribute substantially to the total photo-current.

The measured SPV, presented in figure 7 for the p-Si(111):H surface, becomes unreasonably large for negative sample bias (Hamers *et al.* 1992). The low carrier recombination rate at the p-Si(111):H surface that has no surface states in the

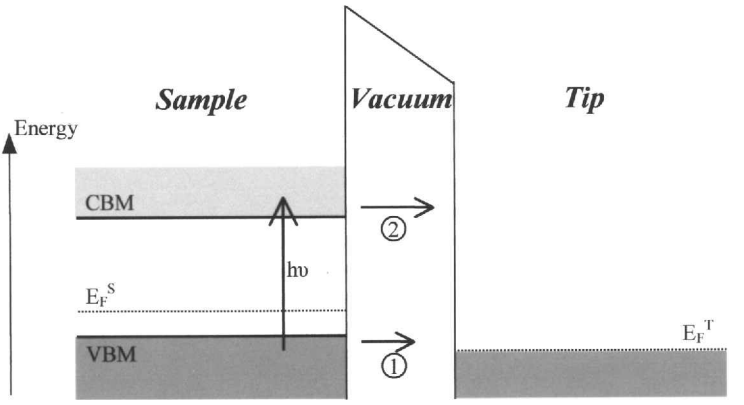

Figure 10. A schematic drawing of a *p*-type semiconductor sample and a tip band diagram for the illustration of a source of photocurrent which does not stem from SPV. The semiconductor bands are shown flat for simplification.

bulk band gap, makes the above mentioned error source plausible. An excess light-enhanced current results in an over-correction of the bias-compensation feedback loop that produces an exaggerated SPV reading. Nevertheless, in our experiments on *p*-GaAs(110) surfaces (Aloni *et al.* 1999), we did not observe any anomalous SPV values, although GaAs(110) surfaces also have a very low surface recombination velocity. We suggest that the reason for this is that the C_3 and C_4 surface resonances that overlap the bulk conduction band and extend into the vacuum, lie 0.6 and 1.1 eV above the CBM, respectively (Chelikowsky and Cohen 1979), and hence cannot be populated with thermalized photo-electrons. Thus, photo-electrons under the *p*-GaAs(110) surface are less available for tunnelling into the tip.

Another source of error that may yield too low SPV readings when using modulated light techniques, is the photovoltage decay time, or the time it takes the bands to resume their original bending in the dark, after the illumination is terminated (see section 2.3). The bias-compensation method can be used if the SPV decays within $< 100\,\mu s$. Naturally, operating at higher light modulation frequencies, which is good to avoid errors due to thermal expansion of the tip and sample, requires a faster SPV decay in the dark (see, for example, Grafstrom *et al.* (1998)).

Generally, whenever a second feedback loop is used to adjust the sample bias so as to maintain a certain tunnelling current upon illumination ($I_t = 0$ in the current-nulling technique) the sensitivity of the current to the bias value should be considered. The slope of the I–V curve determines the accuracy of the feedback loop with which the surface potential is determined. If the I–V curve slope is not symmetric around the working surface voltage, i.e. $d^2I/dV^2 \neq 0$, a consistent error may occur, which is different at various surface locations.

Finally, the effect of a laser optical rectification in the nonlinear tunnelling junction between the sample and the tip has to be considered. Laser-field rectification was observed previously with infrared light (Cutler *et al.* 1987, Volcker *et al.* 1991), and may have a slight contribution to the tunnelling current in the visible-light wavelengths discussed here. While Kuk *et al.* (1990) suggested that a small varying SPV signal of 3–5 mV stems from the rectification effect, time correlated SPV measurements (Hamers and Cahill 1991) ruled it out: no decrease was observed in

the SPV signal for up to 1 ns delay between 1 ps long excitation-laser pulses, with respect to the signal at zero delay.

3. Results of SPV imaging at various surfaces

3.1. *Si*(111)7 × 7 *surfaces*

3.1.1. *Clean Si*(111)7 × 7

Hamers and Markert (1990a, b), immediately followed by Kuk *et al.* (1990, 1991), were the first to use STM for surface photovoltage imaging. Both groups used the current-nulling technique to study the 'metallic' Si(111)7 × 7 surface. The resulting SPV values (positive for *n*-type and negative for *p*-type samples) were constant over the surface within ∼10 mV, except for regions of 15–25 Å in diameter, where the magnitude dropped by ∼95%. The reduced SPV regions could not always be correlated with a topographically-observed defect. Both groups interpreted the reduction in the SPV as due to a local enhancement in the carrier recombination rate. Since most defects and adsorbates at Si(111)7 × 7 surfaces are expected to remove surface states from the bulk band gap, it was suggested that the enhanced local recombination stems from the breaking of the surface symmetry (Hamers and Markert 1990b).

Fine changes in SPV within the 7 × 7 surface unit cell, such as a few mV difference observed between the faulted and the unfaulted halves of the unit cell (Hamers and Market 1990a, b), were also explained by a different recombination rate due to different local densities of filled states next to the Fermi level. Kuk *et al.* (1990), based on a comparison with SPV imaging on a gold surface, suggested that a < 5 mV spatial SPV change that tracks the topography may result from a laser-field rectification effect.

Kochanski and Bell (1992) used a variation on the current-nulling technique, trying to improve the accuracy by extrapolation of the measured *I–V* curves to the zero current point, on clean Si(111)7 × 7 and Si(111):Ge5 × 5 surfaces. Once more, they found the photovoltage to be uniform within 10 mV over a 100 Å range.

Imaging the SPV on Si(111)7 × 7 surfaces under a non-zero electric field between the tip and the sample was performed using the bias-compensation technique (McEllistrem *et al.* 1993). Again, the average observed SPV values were less than 20% of the expected degree of band bending in the dark due to the high carrier recombination velocity at this surface. For all bias values used, the electric field was efficiently screened by the 'metallic' surface, and hence gave rise to a SPV that was independent of the bias (see figure 7). Nevertheless, SPV imaging under a high tip-induced electric field, as presented in figures 11 (*c*) and (*d*) showed a slightly higher (more positive) SPV over the unfaulted half of the 7 × 7 unit cell with respect to the faulted half (McEllistrem *et al.* 1993). According to the DAS model (Takayanagi *et al.* 1985), the unit cell of the Si(111)7 × 7 is divided into two halves, each containing six Si adatoms. When a CCT image is taken at positive sample bias, the Si adatoms in both halves appear at similar heights. However, at negative sample bias, the adatoms at the 'faulted' half appear brighter (higher), possibly due to a higher density of filled states close to the Fermi level. The difference in the observed SPV between the two unit cell halves reveals that the faulted half screens the tip-induced external electric field better than the unfaulted half, which is consistent with a higher density of electrons at the faulted half unit cell. In the case of *p*-type samples, as presented in figure 11, the bands are bent down and the SPV is negative. However,

the field from a negative tip (at positive sample bias) pushes the bands up where the surface fails to screen it fully, making the SPV more positive at the unfaulted half unit cell.

3.1.2. *O–Si*(111)7 × 7

The very initial state of oxygen adsorption on Si(111)7 × 7 surfaces at room temperature appears in CCT STM images as protrusions over the Si adatom sites (Pelz and Koch 1990, Avouris *et al.* 1991). It turns out that these adsorbed oxygen species lower the surface state density next to the Fermi level. As a result, when the STM tip is positioned above such an adsorbed species, an electric field from the tip can penetrate the surface and give rise to band bending which results in a very localized feature in SPV images (McEllistrem *et al.* 1993). Figure 11 shows a contrast in SPV, measured with the bias-compensation technique, which evolved above the 'bright' adsorbed oxygen features at a sample bias of $V_s = +2.0$ V, but not at $V_s = +0.5$ V. We therefore conclude that in the absence of an STM tip, the initial adsorbed mode of oxygen on the Si(111)7 × 7 does not induce any changes in the band bending in its vicinity, rather it lowers the screening ability of the surface locally, on a sub-nanometre scale.

3.1.3. *K–Si*(111)7 × 7 *and Ag–Si*(111)7 × 7

STM images of low coverage potassium at Si(111)7 × 7 surfaces (Hashizume *et al.* 1991a, Gorelik *et al.* 1998) show that single K atoms appear at the surface as missing Si adatoms. The pronounced lowering of the work function due to room temperature potassium adsorption at Si(111)7 × 7 surfaces (Weitering *et al.* 1993), which is linear with K coverage at the low, submonolayer coverage regime, suggests that the adsorbed potassium atom is positively charged. If the charge of a single adsorbed K atom is not compensated fully by a negative charge on the Si atoms directly underneath it, it should give rise to band bending in the vicinity of the K site, which will be manifested in a negative addition to the SPV value. Due to the 'metallic' character of the Si(111)7 × 7 surface, we expect that high lateral screening would limit the area where the bands are bent at the surface to a radius of < 10 Å (see section 4).

A SPV image of the low-coverage K–Si(111)7 × 7 surface (Gorelik *et al.* 1998), using the current-nulling technique, is presented in figure 12; the SPV value around the 'dark' single K-adatom features showed no contrast within the ±2 mV error in the constant SPV = −0.11 V detected (using 0.9 W cm^{-2} of 532 nm light).

SPV images of the low-coverage Ag–*p*-Si(111)7 × 7 surface were obtained by Cahill and Hamers (1991a, b) using the double-modulation technique. The adsorbed silver atoms appeared in CCT images as half unit cell size 'bright' (protruding) islands at 0.02 ML (ML = monolayer) coverage, that grew at higher coverages. Once more, the SPV map did not show any contrast beyond ~3 mV changes that followed the topography at and around the silver islands. Nevertheless, an increase of the average SPV with increasing Ag coverage on *n*-type samples, and a decrease of the SPV with increasing Ag coverage on *p*-type samples, was observed and explained by a coverage dependent change in the Fermi level pinning energy for both doping types, from 0.6 eV above the VBM on the clean surface to 0.4 eV at 1 ML Ag coverage.

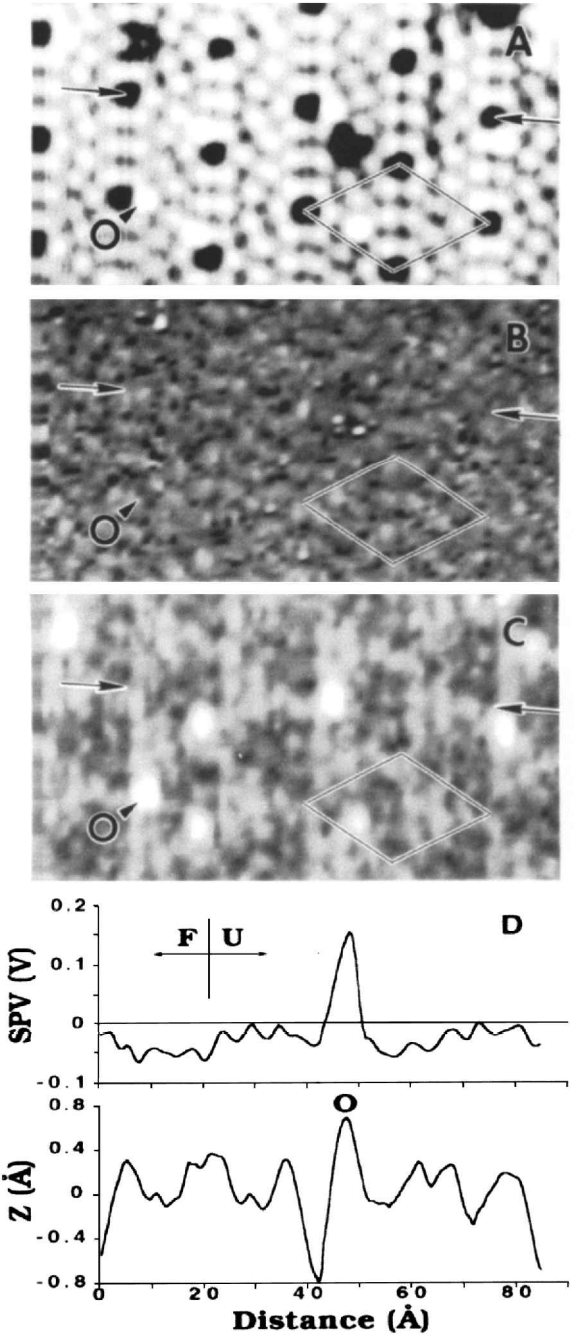

Figure 11. (*a*) A CCT STM image of *p*-Si(111)7 × 7 surface which was exposed to 0.1 L O_2 at room temperature, taken at $V_s = +2.0$ V. (*b*) and (*c*) are SPV images taken simultaneously at $V_s = +0.5$ V and $V_s = +2.0$ V, respectively. (*d*) is a cross-section of both the CCT and the SPV between the two arrows marked in (*a*), (*b*) and (*c*) at $V_s = +2.0$ V (McEllistrem *et al*. 1993).

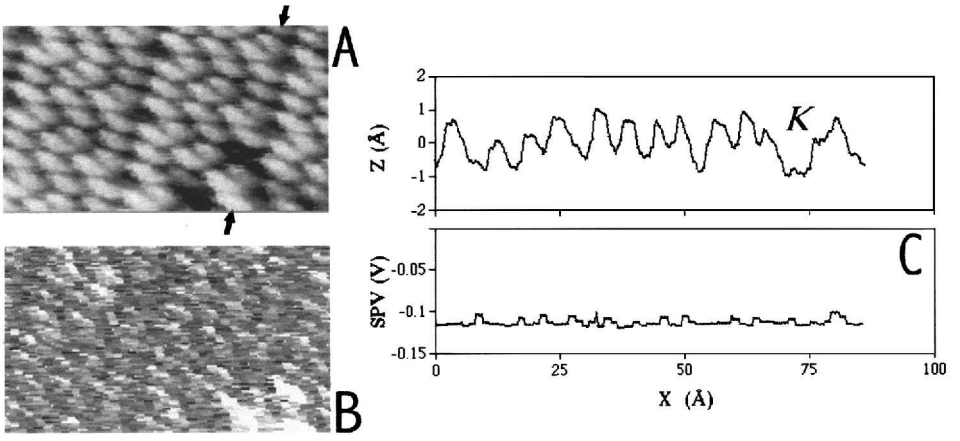

Figure 12. (*a*) CCT image (V_s = −170 mV, I_{tun} = 1 nA) and (*b*) the corresponding SPV image for K–*p*-Si(111)7 × 7 surface. (*c*) is a cross-section taken between the arrows in (*a*), where K denotes the single potassium atom location.

3.2. *Si*(001)2 × 1 *surfaces*

3.2.1. *Clean Si*(001)2 × 1

The Si(001)2 × 1 surface atoms are arranged in dimers that form rows (Hamers *et al.* 1986a). The dimers give rise to a filled π surface band at the top of the valence band and an empty π^* band that occupies the higher energy part of the Si bulk band gap (Himpsel and Fauster 1984, Hamers *et al.* 1987, Hamers and Köhler 1989). The lack of surface states between them results in no Fermi level pinning. Consequently, as explained in section 2.4.2 and shown schematically in figure 8, the electric field from the tip can penetrate the surface and bring about a limited degree of tip-induced band bending. Figure 7 shows the spatially averaged SPV value as a function of the sample bias for both *n*- and *p*-type samples, as was measured using the bias-compensation technique (McEllistrem *et al.* 1993): for *n*-type samples, the bands are always bent upward, giving rise to a positive SPV. At positive sample bias, the bands can be bent further up until the Fermi level meets with the π state, or the VBM, giving rise to a positive SPV that increases with the bias up to a value that equals E_F-VBM. However, at the *p*-Si(001)2 × 1 surface, the bands are free to bend some $\pm$0.2 eV, giving rise to a small value of positive SPV at $V_s > 0$ and negative SPV at $V_s < 0$.

Atomically resolved SPV images, using the current-nulling technique (zero tunnelling current and no potential difference between the surface and the tip) (Kuk *et al.* 1991), showed no features in the SPV map that correspond to the topography image. Other SPV images, such as the one presented in figure 6 (Hamers *et al.* 1992) that was taken using the bias-compensation technique, and the images of Cahill and Hamers (1991a, 1992) using the double-modulation technique (non-zero tunnelling current), showed that a SPV contrast on this surface is detected only on type-B steps and type-C defects which introduce surface states in the energy gap between the π and the π^* bands. The SPV values were current dependent and the features in the SPV map were of sub-nanometre size. No SPV contrast could be detected on missing-dimer defects. SPV imaging as a function of the tunnelling current set point, yielded an estimated lifetime for the injected holes from the tip (at $V_s < 0$)

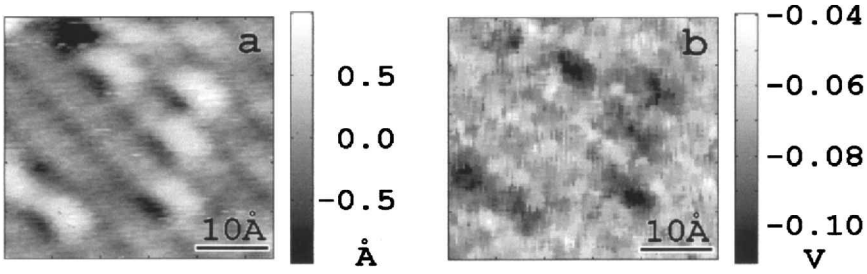

Figure 13. (*a*) CCT and (*b*) SPV images of a Cs–*p*-Si(001)2×1 surface, taken simultaneously at $V_s = -960$ mV, $I_{tun} = 95$ pA.

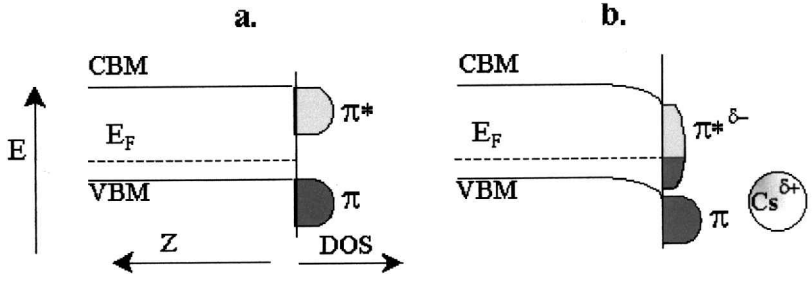

Figure 14. A schematic drawing of the band edges energy (E) as a function of distance into the bulk (z) for: (*a*) a clean portion of the *p*-Si(001)2 × 1 surface, and (*b*) at a Cs-induced feature.

of 10^{-10} s on the Si dimers, while at type-B steps and type-C defects it is larger by a factor of two (Cahill and Hamers 1992).

3.2.2. *Cs–Si*(001)2 × 1

Low coverage Cs adsorption at Si(001)2 × 1 gives rise to features in CCT STM images that involve two adjacent dimers on the same dimer row (Hashizume *et al.* 1991b, Gorelik *et al.* 1999): it seems to occupy an asymmetric valley-bridge position, bound to two dangling bonds of two adjacent dimers, that appear dark (depressed) at negative sample bias images. The two empty dangling bond states on the oposite sides of these dimers appear brighter (higher) at both negative and positive sample bias images. Figure 13 shows a negative sample bias CCT (*a*) and the corresponding SPV (*b*) images for a few Cs adatoms on a *p*-Si(001)2 × 1 surface (Gorelik *et al.* 1999). The SPV images were taken with the bias-compensation technique, giving rise to a SPV value of -55 ± 8 mV at the clean surface (*p*-type material) at $V_s = -0.96$ V (using ~500 mW 532 nm light). Figure 13 (*b*) shows a clear SPV contrast that overlaps the bright unreacted dangling bond features in the CCT image (*a*). We propose that the π^* surface state, due to these two dangling bonds that belong to the two adjacent dimers, is broadened and/or lowered in energy. As a result, a part of this surface state is now positioned below the Fermi level and thus, a negative charge accumulates in it, as can be seen in the schematic band diagram in figure 14. The negative charge compensates the positive charge of the adsorbed Cs atom, yielding a dipole vector with a non-zero component parallel to the surface. This is why the Cs-induced features are oriented in the same direction

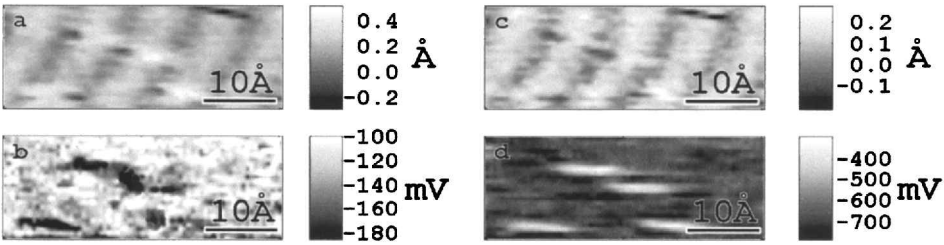

Figure 15. (*a*) and (*c*) CCT and (*b*) and (*d*) SPV images of a Cs–*p*-Si(001)2 × 1 surface, taken simultaneously (every line was repeated at a different bias) at $V_s = -1.1$ V ((*a*) and (*c*)) and $V_s = -2.3$ V ((*b*) and (*d*)), $I_{tun} = 72$ pA.

when they appear close to each other on adjacent dimer rows, or anti-parallel when they appear next to each other on the same row (see figure 13 (*a*)).

If this is the case, we would expect to have a local Fermi level pinning at the site of the altered π^* surface states. Consequently, the SPV contrast above the Cs-feature dangling bonds should change sign when we go from low negative sample bias (small tip-induced downward band bending at clean regions of the surface) to a high negative sample bias (larger tip-induced band bending at clean areas). Figure 15 shows two sets of CCT ((*a*) and (*c*)) and SPV ((*b*) and (*d*)) images which were taken at the same region (repeating each scan line with a different bias) for low ((*a*) and (*b*)) and high ((*c*) and (*d*)) negative sample bias values (Gorelik *et al*. 1999). As expected, the Cs-induced SPV features appeared dark at the low negative sample bias image (*b*) and bright at the high negative sample bias SPV image (*d*). Due to the low density of states in the Cs-induced altered π^* surface states the Fermi level pinning is quite 'soft', hence the SPV values at these features' locations in images 15 (*b*) and (*d*) are not the same. Also the charge on the Cs adatom may change due to the tip-induced electric field. Nevertheless, the fact that the Fermi level is embedded in the Cs-induced Si dangling bond states, which is also why these states appear bright in CCT images at both positive and negative sample bias, is reflected in the bias-dependent contrast of the SPV images.

3.3. *GaAs*(110) *surfaces*

3.3.1. *Clean GaAs*(110)

Clean, defect free GaAs(110) surfaces, which are obtained by cleaving a GaAs wafer that is cut and polished along the (100) plane, have no surface states in the bulk band gap; due to a 1 × 1 reconstruction that causes the As atoms to protrude into the vacuum, the Ga and As dangling bond states become surface resonances that overlap the conduction and the valence bands, respectively (Chelikowsky and Cohen 1979, Zhang and Cohen 1986). As a result, STM CCT images can trace either the Ga or the As sub-lattices at positive or negative sample biases, respectively (Feenstra and Fein 1985, Ebert *et al*. 1996). The lack of surface states makes the surface carrier recombination velocity very low, and hence, a relatively low super-band-gap illumination (400 mW at 532 nm) can nearly flatten the bands (Aphek *et al*. 1998). However, we found that when the average distance between neighbouring steps falls beneath 1000 Å, the observed SPV magnitudes at the clean terraces become smaller for the same illumination intensity. This is possibly due to the high recombination rate at the steps and the large carrier diffusion length in GaAs single crystals.

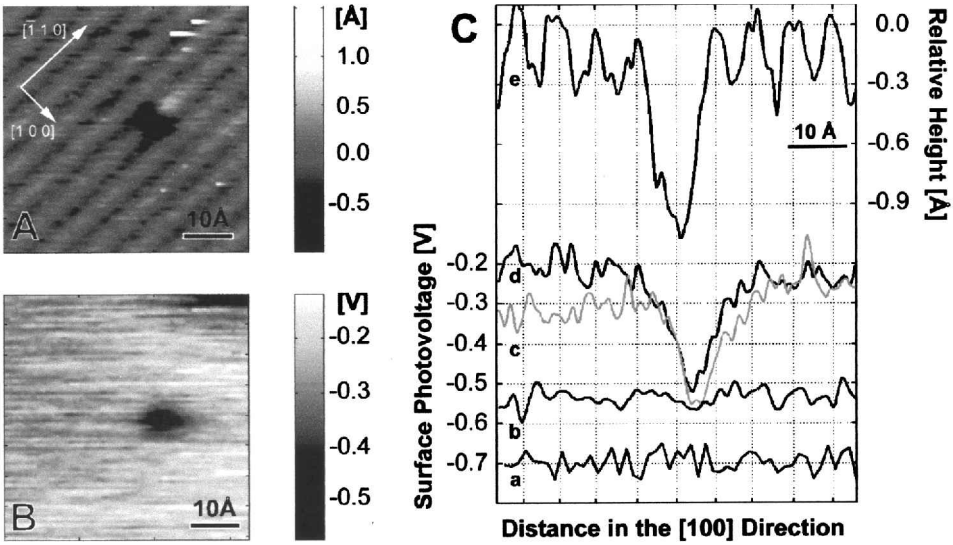

Figure 16. (*A*) Topography and (*B*) SPV images, taken simultaneously at $V_s = -2.8$ V ($I_{tun} = 25$ pA), around an As vacancy, and (*C*) cross-sections in the SPV images along the [100] direction around V_{As}, taken at $V_s = -3.5$ V ($I_{tun} = 29$ pA) (trace a), $V_s = -3.0$ V ($I_{tun} = 18$ pA) (trace b), $V_s = -2.5$ V ($I_{tun} = 29$ pA) (trace c), $V_s = -1.8$ V ($I_{tun} = 30$ pA) (trace d) and $V_s < 0$ (trace e) topography.

Our experiments on clean GaAs(110) surfaces (Aloni *et al*. 1999) were performed with the bias-compensation technique, at tunnelling currents of 20–60 pA. Similarly to Si(111):H (see figures 6 and 7, McEllistrem *et al*. (1993)), the measured SPV was strongly dependent on the tip-induced electric field, but without the anomaly for *p*-type samples at negative sample bias (see section 2.4.3). Spatially averaged SPV versus sample bias curves show a rise in SPV up to a sample bias of 3.5–4 V (for *n*-type samples), above which the SPV magnitude drops. The SPV decrease can be partially explained by a rapid increase of the distance between the tip and the sample as the bias is increased beyond this value, but also by a drop in the SPV due to the penetration of the Fermi level into the valence band (for *n*-type sample).

Arsenic vacancies (V_{As}) at GaAs(110) surfaces appear as dark spots at negative sample bias CCT images (of As-derived filled states), while at positive bias (Ga empty states images) the nearest Ga atoms appear higher (Lengel *et al*. 1994). Recent calculations (Zhang and Zunger 1996, Kim and Chelikowsky 1998) showed that the surrounding Ga atoms may actually be slightly depressed, yet they appear higher due to additional vacancy-derived empty states above them.

Figure 16 shows (*A*) the CCT and (*B*) SPV images of non-degenerate *p*-GaAs(110) surfaces at a sample bias of −2.8 V (Aloni *et al*. 1999), using the bias-compensation technique. Figure 16 (*C*) shows several cross-sections of the SPV images for different values of electric field at the tip–sample junction: as long as the SPV, which reflects the tip-induced band bending far away from the V_{As} site, was small in magnitude (SPV > −0.55 V), the SPV value above the vacancy was pinned at -0.53 ± 0.03 V. However, a larger tip-induced field gave rise to a larger negative SPV which no longer showed Fermi level pinning. For the samples we used (doped $\sim 2 \times 10^{17}$ cm^{-3}), E_F is about 0.09 eV above the VBM in the bulk. Our observations

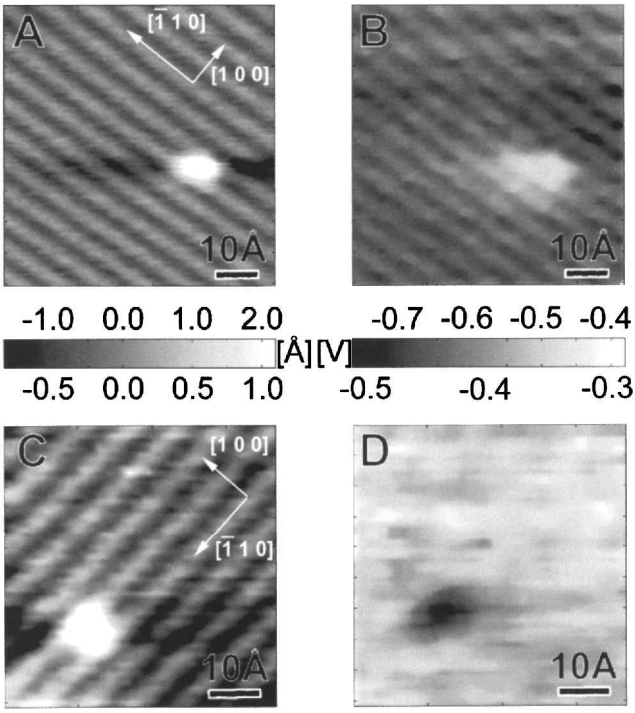

Figure 17. (*a*),(*c*) CCT and (*b*),(*d*) the corresponding SPV images, taken at $V_s = -2.5$ V ($I_{tun} = 29$ pA), of $< 4 \times 10^{12}$ cm^{-2} Cs–*p*-GaAs(110) surface. Images (*a*) and (*b*) were taken with a sharper tip.

imply that at the surface, the Fermi level is free to move from 0.62 ± 0.03 eV above the VBM and up due to external electric fields. Only a filled state in the band gap, which has to be occupied with two electrons to keep the surface neutral, and that extends below ~0.62 eV above the VBM, can give rise to such an effect. Kim and Chelikowsky (1998) indeed predicted a filled state which is centred at approximately 0.2 eV above the VBM, for an As vacancy that is $-1e$ charged (the charge required to maintain this ionic surface neutral). Note also that the minimum in the SPV map does not coincide precisely with the vacancy position, but occurs on the Ga atom row where the dangling bond states reside.

3.3.2. *Cs–GaAs*(110)

Figure 17 shows CCT ((*a*) and (*c*)) and the corresponding SPV ((*b*) and (*d*)) images of a *p*-GaAs(110) sample with single Cs adatoms at a coverage $< 4 \times 10^{12}$ cm^{-2} (Aloni *et al.* 1999). Images 17 (*a*) and (*b*) as well as 17 (*c*) and (*d*) were taken at a sample bias of -2.5 V. However, because the tip had a different shape (or a different composition), the values of the SPV far from the Cs adatoms were different: a sharper tip in 17 (*a*) and (*b*) gave rise to a higher SPV magnitude (*b*) and higher corrugation in the topography (*a*). At the Cs locations, the SPV had a maximum in (*b*) and a minimum in (*d*). Figure 18 shows cross-sections of both the topography (trace h) and SPV images (traces a–g), taken at different sample bias values or tip conditions, around a single Cs atom and along the [100] direction. For clarity, we present only low and high tip-induced field SPV traces, where on clean surface

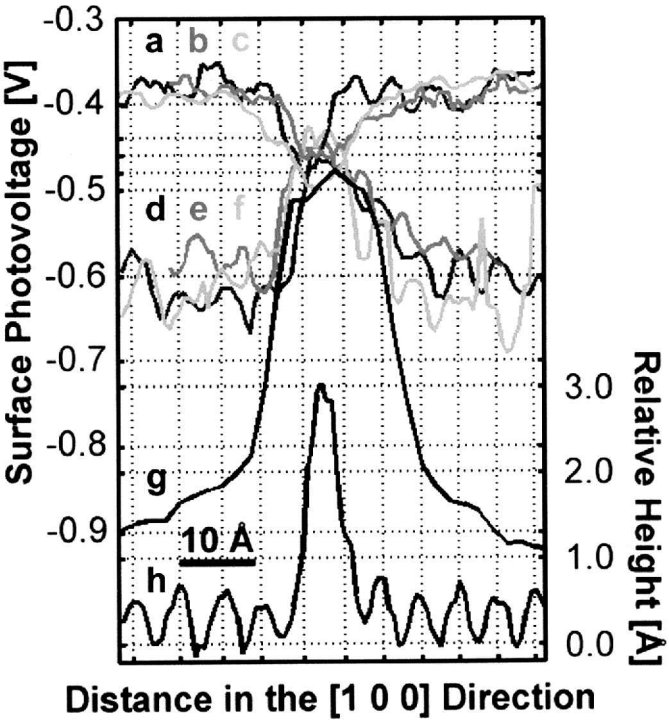

Figure 18. Cross-sections of the SPV images along the [100] direction around a single Cs adatom at the *p*-GaAs(110) sample, taken at traces a and b, $V_s = -1.8$ V ($I_{tun} = 36$ pA), trace c, $V_s = -2.5$ V ($I_{tun} = 29$ pA), trace d, $V_s = -3.0$ V ($I_{tun} = 36$ pA), traces e and f, $V_s = -2.5$ V ($I_{tun} = 29$ pA), trace g, $V_s = -3.6$ V ($I_{tun} = 18$ pA) and trace h, topography at $V_s = -2.5$ V.

regions the SPV values were = −0.4 V (traces a–c) and = −0.55 V (trace d–g), respectively. Above the Cs adatom, traces a–c show a minimum at -0.48 ± 0.03 V while traces d–g show a maximum at -0.45 ± 0.03 V. For the samples we used (doped $\sim 2 \times 10^{17}$ cm^{-3}), the Fermi level is about 0.09 eV above the VBM. Hence, our observations suggest that the Cs adatom contributes a partly-filled surface state which is centred at about 0.56 eV above the VBM (see figure 9).

3.3.3. *O–GaAs*(110)

Single oxygen atoms, adsorbed on an *n*-GaAs(110) surface, appear as a protrusion at negative sample bias, and as a wide (∼50 Å in diameter) indentation at positive sample bias, in STM CCT images (Stroscio *et al*. 1987). The CCT images can be interpreted in terms of an upward band bending around a negatively charged oxygen adatom. This local change of the energy of the band edges at the surface with respect to the Fermi level of the tip, gives rise to a higher overlap of filled states with the tip's empty states for $V_s < 0$, but a lower overlap of empty surface states with filled tip states for $V_s > 0$.

SPV imaging of a low-coverage O/*n*-GaAs(110) surface through the bias compensation technique (Aloni and Haase 1999, 2000) confirms this picture. At a negative sample bias, the SPV was negative, small (< 0.1 V) and featureless. However, at a moderate positive sample bias (1.5–2.5 V), an increase in the tip-induced positive

SPV value was observed locally, and it overlapped spatially the 'dark' topography feature. At no positive sample bias did the contrast in the SPV map around the oxygen adsorbate invert. Unlike the case of a single Cs adatom on GaAs(110) surfaces, which gives rise to a surface state inside the band gap that pins the Fermi level locally, the oxygen adatom does not seem to introduce any surface states in the gap. Instead, the oxygen adsorbate acts as a negative point charge that adds to the electric field from a negative tip (at $V_s > 0$).

3.4. (0001) *surfaces of transition metal dichalcogenides*

Transition metal dichalcogenides are layered materials, where the layers are held by van der Waals forces. The (0001) cleavage plan, parallel to the layers, is characterized by hexagonal array of chemically-saturated chalcogenide atoms and are therefore considered to be inert and free of dangling bonds (Wilson and Yoffe 1968). Hence, like GaAs(110) surfaces, there are no surface states in the bulk band gap and in the absence of charged defects and adsorbates or tip-induced electric field, the bands are supposed to remain flat. The inert nature of these surfaces allows them to remain clean in air.

The only published STM SPV imaging work on a transition metal dichalcogenide surface was done on a WS_2(0001) surface in air by Matthes *et al.* (1998). The samples were *p*-type doped ($10^{17}\,cm^{-3}$) and no tunnelling current could be obtained at negative sample bias, unless the sample was illuminated. Therefore, a photo-induced tunnelling current (PITC) image and a SPV image (using the bias-compensation technique), that were taken at negative sample bias of −0.5 V, had to have the tip-height stabilized in the dark using a positive sample bias at each pixel before the *z*-control feedback was put on hold and the bias was altered to the negative sample bias. Both images showed no contrast on the clean flat terraces, where the measured SPV was 600 mV. However, at a monomolecular step, the SPV value fell to almost zero and so did the PITC. The width of this contrast in the PITC and SPV images was roughly 6 nm. The authors interpreted these results by suggesting that the step introduces surface states into the band gap, which act as a carrier recombination centre that removed the photogenerated minority carrier from the vicinity of the step. Another possible explanation is that the surface states at the step pin the Fermi level close to the valence band. Hence, the tip-induced electric field that bends the bands up on a clean terrace, giving rise to a high value of SPV there, is screened well at the vicinity of the step. Regardless of whether the step is reacted (oxidized) in air, this was the first evidence of the existence of localized surface states introduced to a (0001) surface of a transition metal dichalcogenide crystal.

4. Summary: the source of atomic-size features in SPV images

Originally, the motivation behind the attempt to image local surface photovoltage stemmed from the desire to measure the local degree of band bending around various features, such as charged adsorbates and defects at semiconductor surfaces, in the absence of perturbation from the STM tip. Since the typical screening length of an electric field from a charged surface into the bulk is in the range of 50 to 1000 Å (depending on the dopant concentration), there seems to be no reason for the difficult efforts taken to image the SPV on the atomic size scale. However, when

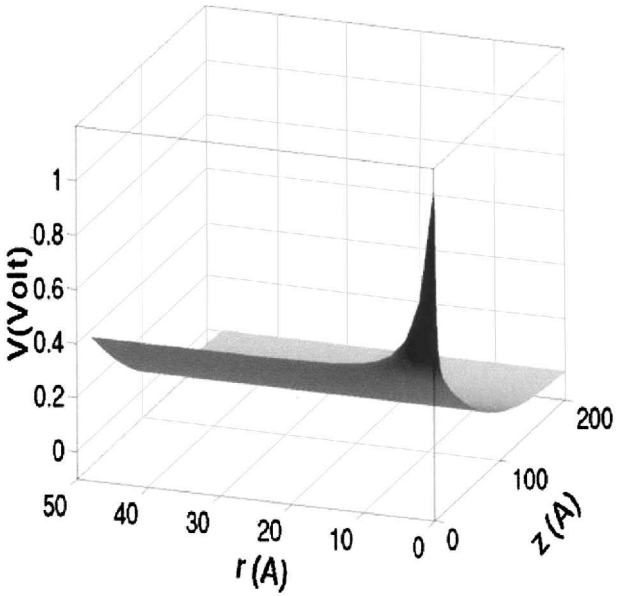

Figure 19. A numerical solution of the Poisson equation for a homogeneous silicon-like matter (*p*-type, 1×10^{17} cm^{-3}), and a half-filled Gaussian DOS in the band gap to represent the 'metallic' 7×7 surface with a single $+1e$ point charge in a 2 Å diameter and 2 Å long cylinder at the origin. **r** is the distance from the charge–dipole at the surface and **z** is the distance into the bulk, while V is the electric potential.

surface states whose energy is inside the bulk band gap limit the Fermi level energy at the surface, the local change in the degree of band bending can be laterally confined to much smaller radii.

A good example is that of a point charge (say, a single positively-charged adsorbed alkali metal atom) on a Si(111)7×7 surface which has a high density of surface state bands covering the bulk energy gap. Figure 19 shows a solution of the Poisson equation in cylindrical coordinates for a $+1e$ charge in a 2 Å long cylinder of 2 Å in diameter, positioned 2 Å above a *p*-Si(111)7×7-like 'smooth' surface (doping level of 1×10^{17} cm^{-3}); the density of surface states versus energy curve is simplistically represented everywhere at the surface by a Gaussian which is centred in mid-gap and defined electrically neutral when half filled. The coordinate **z** denotes the distance from the surface into the bulk (which is kept at an electrical potential 0) and the coordinate **r** represents the lateral distance from the charged cylinder, parallel to the surface. At large r, one can see a downward band bending (seen here as an upward potential change) as a result of Fermi level pinning close to the middle of the surface DOS on a clean surface. Closer to $r = 0$, a sharp increase of the band bending results from the charged 'adsorbate'. Due to the metallic character of the Si(111)7×7 -like surface, which gives rise to a short lateral screening length, the extra local band bending decreases rapidly with r; it reduces to 10% of the clean surface band bending at a radius of about 7 Å away from the charged spot. On the real Si(111)7×7 surface, this is about the average distance between neighbouring Si adatoms. Moreover, because the partly-filled Si-adatom dangling bond state (S_1) is responsible for the surface metallicity, the local band bending is expected to be even

more pronounced locally, between the charged adsorbate and its nearest-neighbour Si adatoms.

However, SPV images taken around a single potassium (Gorelik *et al.* 1998) or oxygen (McEllistrem *et al.* 1993) adsorbate at Si(111)7 × 7 samples in the limit of zero electric field between the tip and the sample (see figure 12 and figure 11 (*b*), respectively) showed no SPV contrast. This may be due to the fact that the adsorbate charge is fully compensated by a silicon atom in its close vicinity, thus avoiding a net electric field that would be screened by carriers at a larger distance. Hence the only SPV contrast that was observed at the Si(111)7 × 7 surface and had a size of 15–25 Å was attributed to a local higher surface recombination rate due to surface defects that break the surface symmetry (Hamers and Markert 1990a, b, Kuk *et al.* 1990, 1991). Nevertheless, one should bear in mind that the carrier diffusion length in the studied semiconductors exceeds 1000 Å and hence a very efficient recombination centre should drain the photogenerated minority carrier concentration in the sub-surface region on a larger distance scale. Also, most defects and oxygen adsorption modes at the Si(111)7 × 7 surface tend to reduce the surface recombination velocity because they remove surface states from the bulk band gap (Hamers and Markert 1990a, b).

Other observed sub-nanometre size SPV features stem from the influence of the STM tip on the band bending. Different rates of charge transfer between various surface states and the bulk electronic bands gives rise to different amounts of accumulated charge under the STM tip apex. The different charge, in turn, results in different degrees of tip-induced band bending that leads to a contrast in the SPV which is tunnelling current dependent (see figure 6) (Cahill and Hamers 1991a, 1992, Hamers *et al.* 1992).

When the tunnelling current is kept low enough to avoid effective charging under the tip's apex, one can discern a clear effect of the sample bias on the magnitude of localized sub-nanometre scale SPV features. The bias effect, or the phenomenon of tip-induced electric field penetration through the surface, was demonstrated at two types of surfaces: one type is a metallic surface, such as the Si(111)7 × 7 surface. Here, the surface screens the external electric field well, except at the location of an adsorbate that removes the screening surface states locally, where tip-induced band bending can occur (see figure 11). The other type of surface has an energy gap around the Fermi level position, thus allowing an external electric field from the tip to bend the bands and yield a bias (or tip shape) dependent SPV everywhere. Single adsorbates or single missing atom defects that give rise to a localized surface state, and hence pin the Fermi level locally, can bring about a sub-nanometre SPV contrast that is *not* sample-bias dependent (see figures 9, 13, 15, 16, 17 and 18).

Finally, atomically-resoved patterns in the SPV map that follow closely the clean surface topography and whose magnitude is smaller than 10 mV, were explained in various ways. First, the accuracy of the SPV measurements that rely on the tunnelling current as a measure of the surface potential has to be considered. Different values of d^2I/dV^2 can give rise to different magnitudes of a systematic error on top of different surface sites, in the determination of the precise SPV values. Second, surface charging due to a non-zero tunnelling current, as well as the penetration of the tip-induced electric field can vary slightly with the varying local density of surface states on top and between atoms on the clean and perfect surface. Even when using the current-nulling technique, the zero-current set point may be

slightly offset (Kuk *et al*. 1990), or the contact potential difference between the tip and the surface, due to their different work function values, may give rise to a finite electric field in the vacuum gap between them. Third, a laser rectification effect in the nonlinear tip–sample junction may have a slight contribution to the tunnelling current under illumination as well, that follows the surface morphology (Cutler *et al*. 1987, Kuk *et al*. 1990, Volcker *et al*. 1991).

In conclusion, it was demonstrated that SPV imaging with STM can detect local band bending, local screening capabilities and local charge-carrier dynamics at semiconductor surfaces. If the different effects that give rise to atomically-resolved features in the SPV images can be isolated through a careful study of the contributions due to tunnelling current and sample bias, and maybe also the illumination wavelength (pumping carriers from or into specific surface states with sub-band-gap energy photons (Richter *et al*. 1990)), SPV imaging may prove to be very fruiful in elucidating the nature of various defect- and adsorbate-induced surface states. Obtaining SPV maps together with STM CCT images can lead to a better understanding of both the thermal- and the photo-reactivity towards chemical processes at semiconductor surfaces, as well as provide tools for detailed analysis of microelectronics devices.

Acknowledgements

I wish to thank Professor R. J. Hamers, from the University of Wisconsin in Madison, USA, who introduced me to scanning tunnelling microscopy and surface photovoltage imaging. Much of the material covered in this review is based on very illuminating discussions with him. I also wish to emphasize the contribution of Dr McEllistrem who was a graduate student with Professor Hamers during the year that I spent in Madison, and Mr Shaul Aloni who is a very capable graduate student in my group at the Weizmann Institute in Israel.

Some of this work was supported by the Israeli Science Foundation and by a grant from the Angel Faivovich Fund for Scientific Research.

References

Aloni, S., and Haase, G., 1999, *J. Vac. Sci. Technol.* B., **17**, 2651.
Aloni, S., and Haase, G., 2000, in preparation.
Aloni, S., Nevo, I., and Haase, G., 1999, *Phys. Rev.* B, **60,** 2165.
Aphek, O. B., Kronik, L., Leibovitch, M., and Shapira, Y., 1998, *Surf. Sci.*, **409,** 485.
Avouris, P., Lyo, I.-W., and Bozso, F., 1991, *J. Vac. Sci. Technol.* B, **9,** 424.
Bardeen, J., 1947, *Phys. Rev.*, **71,** 717.
Cahill, D. G., and Feenstra, R. M., 1993, *J. Vac. Sci. Technol.* A, **11,** 792.
Cahill, D. G., and Hamers, R. J., 1991a, *J. Vac. Sci. Technol.* B, **9,** 564.
Cahill, D. G., and Hamers, R. J., 1991b, *Phys. Rev.* B, **44,** 1387.
Cahill, D. G., and Hamers, R. J., 1992, *Scanning Microsc.*, **6,** 931.
Chelikowsky, J. R., and Cohen, M. L., 1979, *Phys. Rev.* B, **20,** 4150.
Cutler, P. H., Feuchtwang, T. E., Tsong, T. T., Nguyen, H., and Lucas, A. A., 1987, *Phys. Rev.* B, **35,** 7774.
Darling, R. B., 1991, *Phys. Rev.* B, **43,** 4071.
Dember, H., 1931, *Phys. Zeit.*, **32,** 554; 856.
Demuth, J. E., Thompson, W. J., DiNardo, N. J., and Imbihl, R., 1986, *Phys. Rev. Lett.*, **56,** 1408.
Ebert, P., Engels, B., Richard, P., Schroeder, K., Blugel, S., Domke, C., Heinrich, M., and Urban, K., 1996, *Phys. Rev. Lett.*, **77,** 2997.
Feenstra, R. M., and Fein, A. P., 1985, *Phys. Rev.* B, **32,** 1394.
Feenstra, R. M., and Stroscio, J. A., 1987, *J. Vac. Sci. Technol.* B, **5,** 923.
Gadzuk, J. W., 1999, *J. Electron. Spectrosc. Relat. Phenom.*, **99,** 321.

GARRETT, C. G. B., and BRATTAIN, W. H., 1955, *Phys. Rev.*, **99,** 376.
GLEMBOCKI, O. J., SNOW, E. S., MARRIAN, C. R. K., PROKES, S. M., and KATZER, D. S., 1992, *Ultramicroscopy*, **42–44,** 764.
GORELIK, D., ALONI, S., EITLE, J., MEYLER, D., and HAASE, G., 1998, *J. chem. Phys.*, **108,** 9877.
GORELIK, D., ALONI, S., and HAASE, G., 1999, *Surf. Sci.*, **432,** 265.
GRAFSTROM, S., SCHULLER, P., KOWALSKI, J., and NEUMANN, R., 1998, *J. appl. Phys.*, **83,** 3453.
GÜNTHERODT, H.-J., and WIESENDANGER, R. (eds), 1994, *Scanning Tunneling Microscopy I. Surface Sciences* (Heidelberg: Springer Verlag).
HAMERS, R. J., and CAHILL, D. G., 1991, *J. Vac. Sci. Technol.* B, **9,** 514.
HAMERS, R. J., HAASE, G., and MCELLISTREM, M., 1992, unpublished results.
HAMERS, R. J., and KÖHLER, U. K., 1989, *J. Vac. Sci. Technol.* A, **7,** 2854.
HAMERS, R. J., and MARKERT, K., 1990a, *J. Vac. Sci. Technol.* A, **8,** 3524.
HAMERS, R. J., and MARKERT, K., 1990b, *Phys. Rev. Lett.*, **64,** 1051.
HAMERS, R. J., TROMP, R. M., and DEMUTH, J. E., 1986a, *Phys. Rev.* B, **34,** 5343.
HAMERS, R. J., TROMP, R. M., and DEMUTH, J. E., 1986b, *Phys. Rev. Lett.*, **56,** 1972.
HAMERS, R. J., TROMP, R. M., and DEMUTH, J. E., 1987, *Surf. Sci.*, **181,** 246.
HASHIZUME, T., MOTAI, K., HASEGAWA, Y., SUMITA, I., TANAKA, H., AMANO, S., HYODO, S., and SAKURAI, T., 1991a, *J. Vac. Sci. Technol.* B, **9,** 745.
HASHIZUME, T., SUMITA, I., MURATA, Y., HYODO, S., and SAKURAI, T., 1991b, *J. Vac. Sci. Technol.* B, **9,** 742.
HECHT, M. H., 1990, *Phys. Rev.* B, **41,** 7918.
HIGASHI, G. S., CHABAL, Y. J., TRUCKS, G. W., and RAGHAVACHARY, K., 1990, *Appl. Phys. Lett.*, **56,** 656.
HIMPSEL, F. J., and FAUSTER, T., 1984, *J. Vac. Sci. Technol.* A, **2,** 815.
HIMPSEL, F. J., HOLLINGER, G., and POLLACK, G., 1983, *Phys. Rev.* B, **28,** 7014.
JOHNSON, E. O., 1958, *Phys. Rev.*, **111,** 153.
KIM, H., and CHELIKOWSKY, J. R., 1998, *Surf. Sci.*, **409,** 435.
KOCHANSKI, G. P., and BELL, R. F., 1992, *Surf. Sci.*, **273,** L435.
KRONIK, L., and SHAPIRA, Y., 1999, *Surf. Sci. Rep.*, **37**, p. 1.
KUK, Y., BECKER, R. S., SILVERMAN, P. J., and KOCHANSKI, G. P., 1990, *Phys. Rev. Lett.*, **65,** 456.
KUK, Y., BECKER, R. S., SILVERMAN, P. J., and KOCHANSKI, G. P., 1991, *J. Vac. Sci. Technol.*, **9,** 545.
LENGEL, G., WILKINS, R., BROWN, G., WEIMER, M., GRYKO, J., and ALLEN, R. E., 1994, *Phys. Rev. Lett.*, **72,** 836.
MATTHES, T. W., SOMMERHALTER, C., RETTENBERGER, A., BÖHMISCH, M., BONEBERG, J., LUX-STEINER, M. C., and LEIDERER, P., 1998, *Appl. Surf. Sci.*, **123–124,** 187.
MCELLISTREM, M., HAASE, G., CHEN, D., and HAMERS, R. J., 1993, *Phys. Rev. Lett.*, **70,** 2471.
MILLS, A., and LE HUNTE, S., 1997, *J. Photochem. Photobiol.* A, **108,** 1.
MOENCH, W., 1993, *Semiconductor Surfaces and Interfaces* (Berlin: Springer Verlag).
PELZ, J. P., and KOCH, R. H., 1990, *Phys. Rev.* B, **42,** 3761.
PICHAT, P., and FOX, M. A., 1988, *Photoinduced Electron Transfer*, Part D, edited by M. A. Fox and M. Chanon (Amsterdam: Elsevier), p. 241.
RICHTER, L. J., BUNTIN, S. A., KING, D. S., and CAVANAGH, R. R., 1990, *Phys. Rev. Lett.*, **65,** 1957.
STROSCIO, J. A., FEENSTRA, R. M., and FEIN, A. P., 1987, *Phys. Rev. Lett.*, **58,** 1668.
SZE, S. M., 1981, *Physics of Semiconductor Devices* (New York: Wiley).
TAKAYANAGI, K., TANISHIRO, Y., TAKAHASHI, M., and TAKAHASHI, S., 1985, *Surf. Sci.*, **164,** 367.
TAMM, I. E., 1932, *Phys. Z. Sowjetumim.*, **1,** 733.
TROMP, R. M., HAMERS, R. J., and DEMUTH, J. E., 1986, *Phys. Rev.* B, **34,** 1388.
VOLCKER, M., KRIEGER, W., SUZUKI, T., and WALTHER, H., 1991, *J. Vac. Sci. Technol.* B, **9,** 541.
WEIMER, M., KRAMAR, J., and BALDESCHWIELER, J. D., 1989, *Phys. Rev.* B, **39,** 5572.
WEITERING, H. H., CHEN, J., DINARDO, N. J., and PLUMMER, E. W., 1993, *Phys. Rev.* B, **48,** 8119.
WILSON, J. A., and YOFFE, A. D., 1968, *Adv. Phys.*, **18,** 193.
ZHANG, S. B., and COHEN, M. L., 1986, *Surf. Sci.*, **172,** 754.
ZHANG, S. B., and ZUNGER, A., 1996, *Phys. Rev. Lett.*, **77,** 119.